Diurnal Patterns of Rainfall in Northwestern South America. Part I: Observations and Context

BRIAN E. MAPES

NOAA–CIRES Climate Diagnostics Center, Boulder, Colorado

THOMAS T. WARNER AND MEI XU

Program in Atmospheric and Oceanic Sciences, University of Colorado, and Research Applications Program, National Center for Atmospheric Research, Boulder, Colorado*

ANDREW J. NEGRI

NASA Goddard Space Flight Center, Laboratory for Atmospheres, Greenbelt, Maryland

(Manuscript received 10 January 2002, in final form 29 August 2002)

ABSTRACT

One of the rainiest areas on earth, the Panama Bight and Pacific (western) littoral of Colombia, is the focal point for a regional modeling study utilizing the fifth-generation Pennsylvania State University–NCAR Mesoscale Model (MM5) with nested grids. In this first of three parts, the observed climatology of the region is presented. The seasonal march of rainfall has a northwest–southeast axis, with western Colombia near the center, receiving rain throughout the year. This study focuses on the August–September season. The diurnal cycle of rainfall over land exhibits an afternoon maximum over most of South and Central America, typically composed of relatively small convective cloud systems. Over some large valleys in the Andes, and over Lake Maracaibo, a nocturnal maximum of rainfall is observed. A strong night/morning maximum of rainfall prevails over the coastal ocean, propagating offshore and westward with time. This offshore convection often takes the form of mesoscale convective systems with sizes comparable to the region's coastal concavities and other geographical features. The 10-day period of these model studies (28 August–7 September 1998) is shown to be a period of unusually active weather, but with a time-mean rainfall pattern similar to longer-term climatology. It is concluded that the rain-producing processes during this time period are likely to be typical of those that shape the seasonal climatology.

1. Introduction

The highest annual rainfall in the Americas, and among the highest in the world, is observed in western Colombia, on the Pacific coastal plain west of the Andes (Eslava 1994; Horel and Cornejo-Garrido 1986; Figueroa and Nobre 1990; Mesa et al. 1997; Poveda and Mesa 2000). Just offshore, where the climatological intertropical convergence zone (ITCZ) meets the coast of western Colombia in a concavity designated the Panama Bight by Nichols and Murphy (1944), a striking maximum appears in remotely sensed convection climatologies of various kinds (e.g., Meisner and Arkin 1987; Garreaud and Wallace 1997; Adler et al. 2000), as well as in many models. Velasco and Fritsch (1987) showed that this area of western Colombia, onshore and offshore, has an anomalously large number of mesoscale convective complexes (MCCs), with most occurring in boreal summer. A dramatic north–south gradient over just a few hundred kilometers separates some of the earth's wettest places from some of its driest, the coastal deserts of Ecuador and Peru (Trewartha 1981; Snow 1976). This gradient roughly parallels the steep sea surface temperature gradient between the equatorial cold tongue and warmer waters to the north.

Because of the small scales involved in convective rainfall, and its dependence on sharp geographical elements such as coastlines and mountains, the study of climate in this complex region requires high spatial resolution. Convection also exhibits strong diurnal modulation, so high time resolution (hours) is also required. Steep, high topography and heavily and diversely vegetated land surfaces must be accounted for in models.

* The National Center for Atmospheric Research is partially sponsored by the National Science Foundation.

Corresponding author address: Brian Mapes, CIRES, 216 UCB, Boulder, CO 80309-0216.
E-mail: bem@cdc.noaa.gov

© 2003 American Meteorological Society

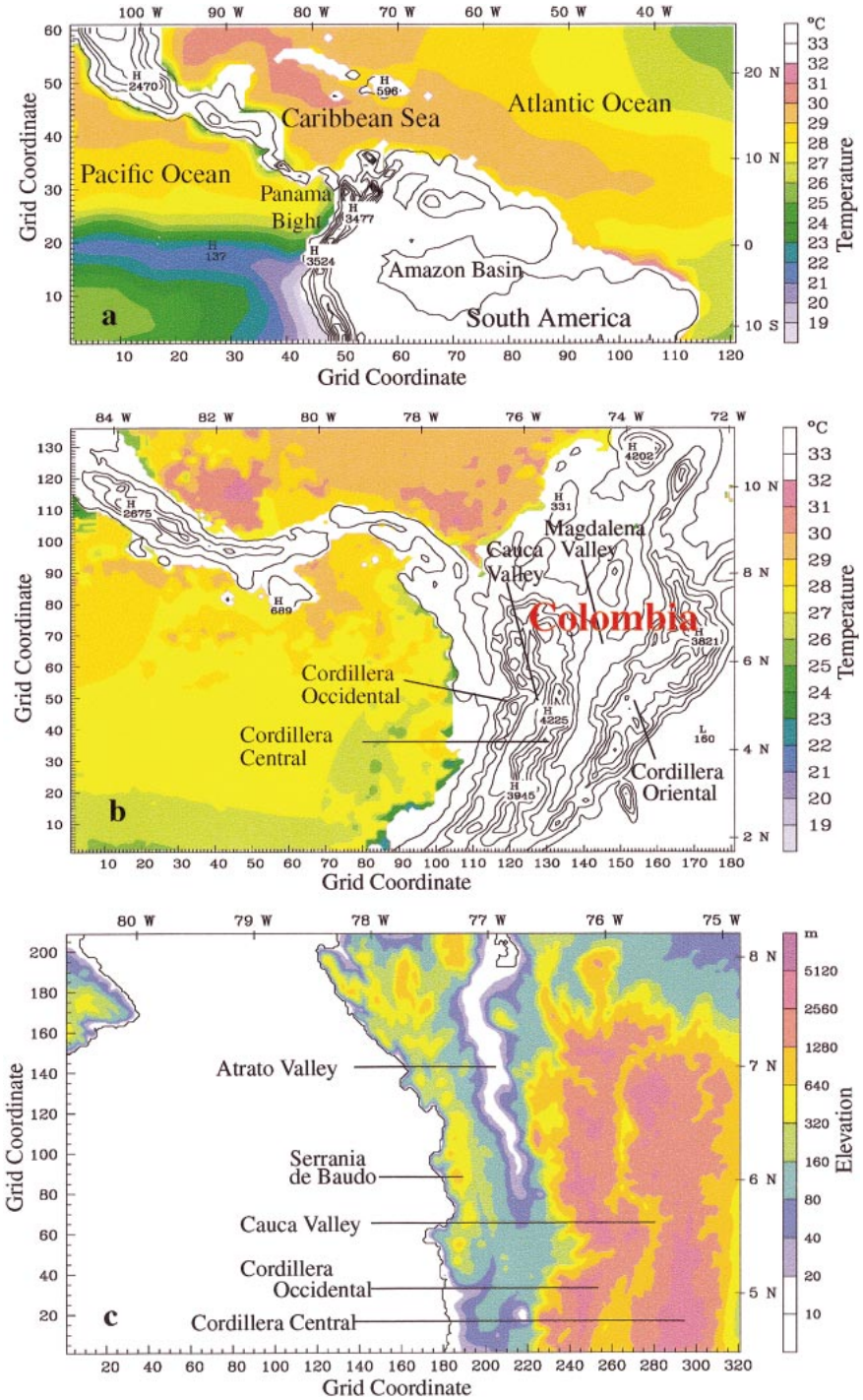

FIG. 1. Terrain elevation and SST for (a) model grid 1, (b) model grid 3, and (c) terrain elevation for grid 4. The terrain contour interval for grids 1 and 3 is 600 m. The grid-4 terrain is color-banded at an irregular interval. The SST is color-banded at an interval of 1°C. Low values along the coasts in (a) are artifacts of the dataset.

Observations must sample land and ocean areas even-handedly and throughout the day.

With these challenges in mind, we have undertaken an investigation of the physical processes behind the rainfall climate in this region. Our main tools are previously published local observations, satellite data, and the fifth-generation Pennsylvania State University–National Center for Atmospheric Research (Penn State–

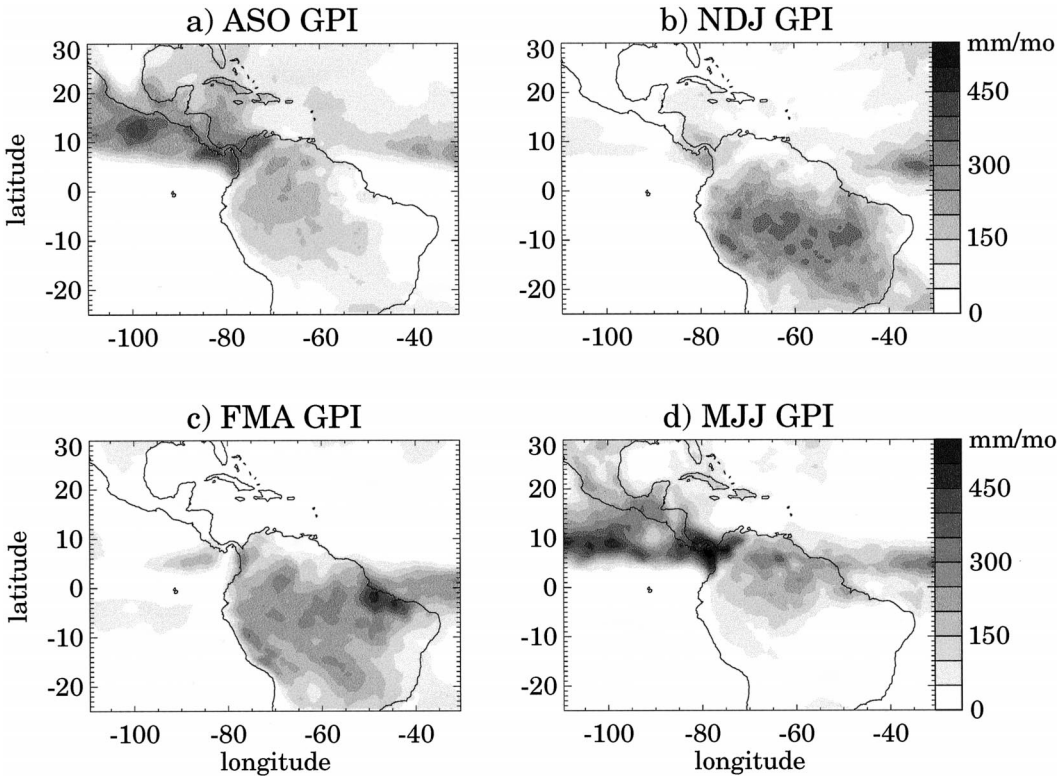

FIG. 2. Mean seasonal march of GPI rainfall estimate in the 1998–99 dataset. Shading density is linearly proportional to rainfall: (a) Aug–Oct, (b) Nov–Jan, (c) Feb–Apr, and (d) May–Jul.

NCAR) Mesoscale Model (MM5) system, described in more detail in Warner et al. (2003, Part II). Figure 1 illustrates the basic geography of the region, with topography indicated as it is represented in the model, and sea surface temperature conditions for the time of our simulations (August–September 1998; see Part II for details regarding SST data). The Andes Mountains lie along the western edge of South America, and branch out at their northern end, in the nation of Colombia, to define several large valleys. Highlands continue through Central America, with notable gaps at the Panama Canal (9°N, 80°W), Lake Nicaragua (11°N, 85°W), and at the Gulf of Tehuantepec (15°N, 95°W). The Guiana Highlands near 5°N, 50°–70°W define the northern edge of the Amazon basin. The cold tongue of the equatorial eastern Pacific (Fig. 1a) had temperatures as low as 22°C (anomalously warm, in the late stages of the 1997–98 El Niño). In general SST was above 27°C throughout the Caribbean Sea, and the western Atlantic and eastern Pacific Oceans. Low values at the coasts in Fig. 1 are artifacts of interpolation, superceded on domain 3 by the satellite-derived sea surface temperatures shown in Fig. 1b.

The results of this research effort are presented in this three-part series. Part I (this paper) describes the observational and historical context and background for the 10-day simulations. Part II (Warner et al. 2003) describes our quest for a satisfactory control simulation, sufficiently accurate that the physical processes diagnosed from the control and sensitivity experiments are credible as representations of nature. Part III (Mapes et al. 2003) describes the physical processes behind nocturnal convection offshore, as revealed by the model. In the present paper, after a historical review (section 2), satellite data are described (section 3) and used, in concert with wind analyses, to depict the regional seasonal climatology (section 4). Section 5 discusses the rainfall climatology and diurnal cycle in western Colombia in particular. Section 6 compares the 10-day time period of our model simulations to climatology.

2. Historical background

The contrasting climates of northern South America have intrigued geographers and meteorologists for many decades [Trewartha (1981), Snow (1976), and Forsbergh (1969) have extensive bibliographies of older sources]. Surface observations at land sites have long been sufficient to elucidate the general pattern of rainfall in the tropical Americas, with abundant rainfall in Central America and Colombia giving way to much drier conditions along the Pacific coast near and south of the equator. The basic annual and diurnal cycles may be summarized to a first approximation as rain (over tropical land) tending to follow the sun, with some time lag.

The annual lag between sun and rain may be a month

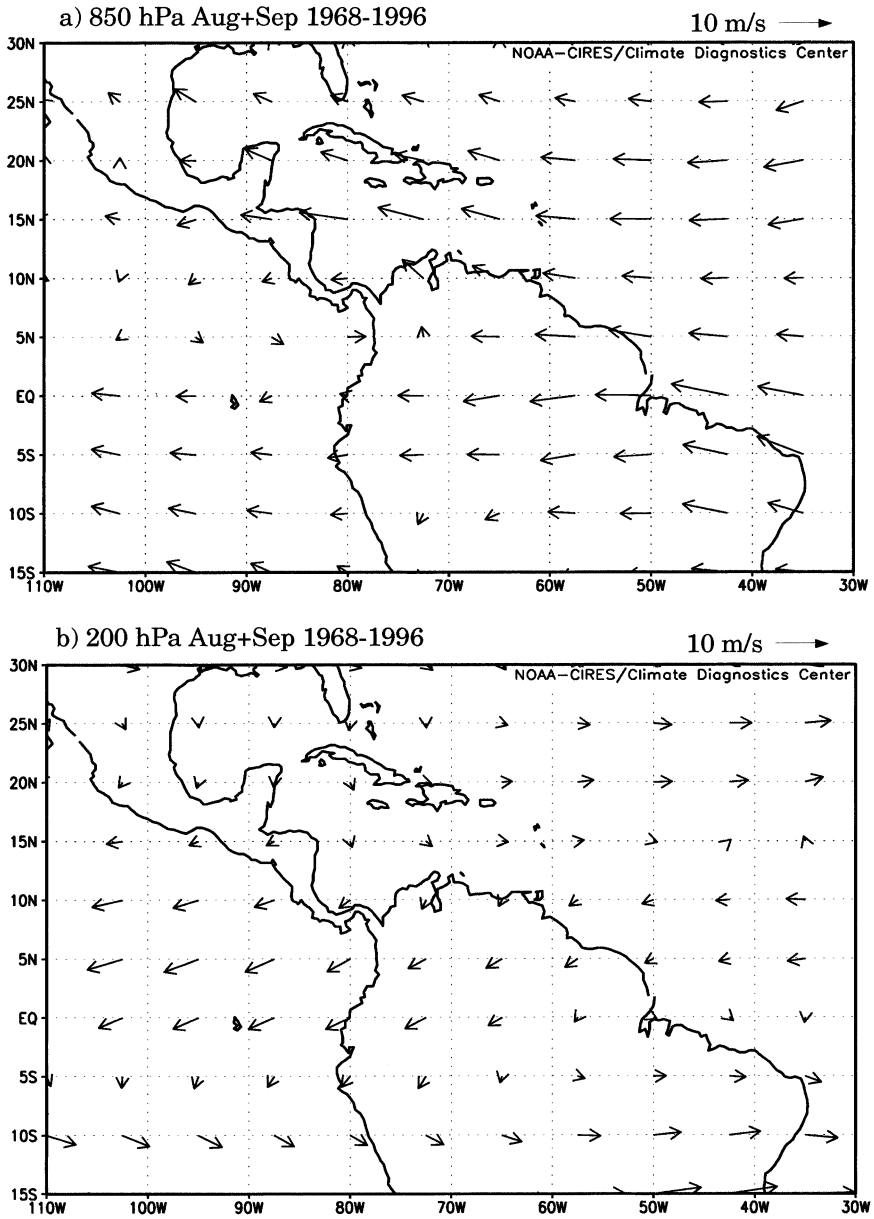

FIG. 3. Climatological (1968–96) Aug + Sep mean wind vectors, from NCEP–NCAR reanalysis data at (a) 850 and (b) 200 hPa.

or more, consistent with a hemispheric-scale heat capacity involving the upper ocean. According to the Climate Prediction Center (CPC) Merged Analysis of Precipitation (CMAP; Xie and Arkin 1996) for 1979–2001, the annual harmonic of rainfall for the Northern Hemisphere American Tropics has its peak near 1 August, while the annual harmonic of Southern Hemisphere precipitation, even over land (interior Amazonia), has its peak in late January, well after the December solstice. The much shorter diurnal lag between sun and rain over land reflects the much smaller thermal inertia of land and the atmospheric boundary layer, as most tropical land areas have their maximum precipitation in the afternoon and evening.

The extreme annual rainfall of Pacific Colombia is due to the fact that, centered at 5°N, it sits near the hub of the annual march, and receives rainfall throughout the year (see, e.g., Fig. 2): over 300 days per year at Andagoya, Colombia (5°N, 77°W) for example (Day 1926). The diurnal variation in this area has a peculiar aspect, as noted in a 1930 German-language paper by Knoch quoted in Trewartha (1981). Along the coast, most rain falls at night, as a steady rain. This is distinguished from the rains farther inland, which peak in the

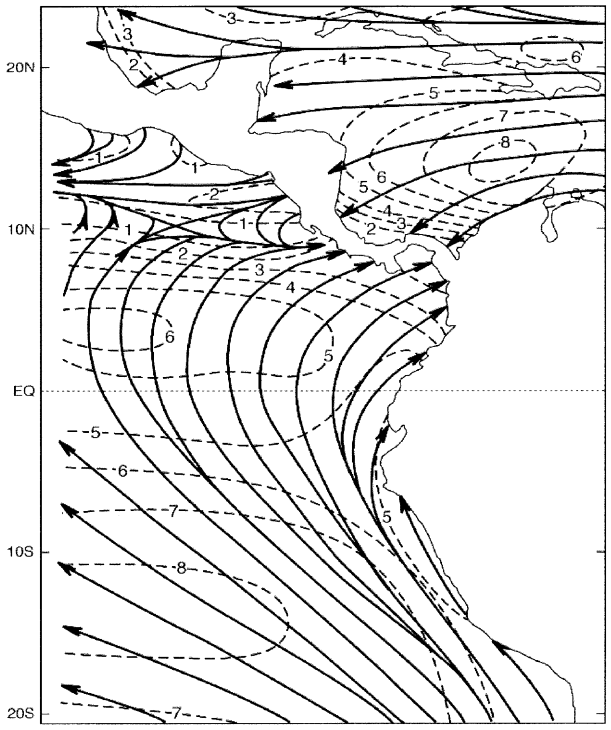

FIG. 4. The Sadler (1986) Aug mean surface wind climatology. Isotachs in m s^{-1} (dashed contours).

afternoon and fall as ''heavy showers and cloud-bursts.'' This observation might suggest a propagating component to the diurnal cycle, with convection initiated over land in the afternoon and perhaps developing into propagating long-lived storms that can yield a nocturnal diurnal peak in adjacent regions. Propagating diurnal cycles are seen in other parts of the world, including the United States in summer (e.g., Wallace 1975; Carbone et al. 2002), and in Asia (e.g., Satomura 2000; Yang and Slingo 2001; Ohsawa et al. 2001; Zuidema 2003).

The advent of satellite remote sensing and global analysis has yielded a more complete picture of the convective climatology of the tropical Americas (Horel et al. 1989; Negri et al. 1994; Garreaud and Wallace 1997). In addition to mean cloudiness fields, the mesoscale convective systems that make up the convective cloudiness have been the object of special study, based on connected structures seen in infrared satellite imagery (Velasco and Fritsch 1987; Machado et al. 1998). In this paper, satellite rainfall estimates of unprecedented detail are shown for the year 2000, along with more standard geostationary estimates for the year of our simulations (1998).

3. Data and methods

Rainfall is the main variable of interest in this study, because it is a major variable in the hydrologic cycle, and because it is a convenient two-dimensional ground-level field summarizing important aspects of the unobservable three-dimensional complexities of convection. Unfortunately, observations of convective rainfall are difficult, so indirect proxy measurements must be used. Infrared images of cold cloudiness have good resolution and uniform coverage, but are only indirectly related to rain. On the other hand, microwave remote sensing (both passive and active) can detect raindrops more directly, but has poorer space–time sampling and different response characteristics over land and sea. A promising strategy has been to use the more direct measurements—rain gauges and microwave rainfall estimates—to calibrate rain-rate estimates from the better-sampled infrared cloudiness data. A variety of techniques, with different levels of complexity, have been used (e.g., Arkin and Meisner 1987; Adler et al. 2000; Sorooshian et al. 2000; Negri et al. 2002). For present purposes, we choose the simplest [Geostationary Operational Environmental Satellite (GOES) Precipitation

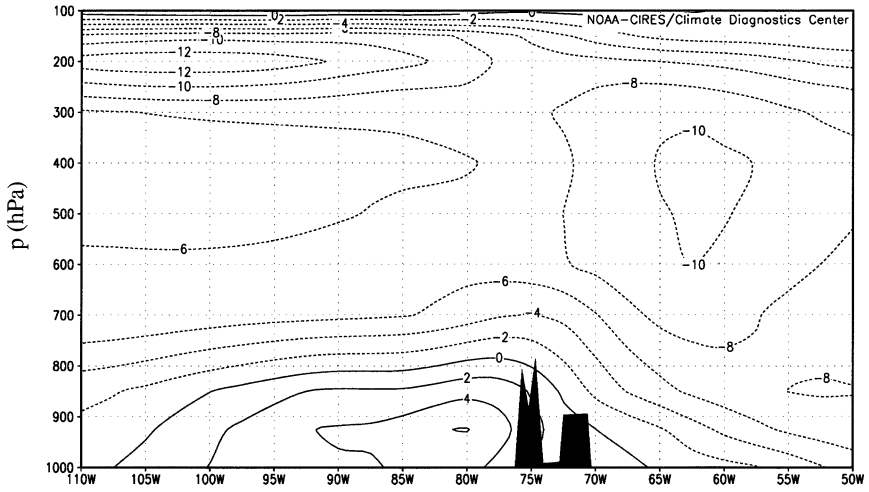

FIG. 5. Climatological (1968–96) Aug + Sep mean zonal wind cross section along 5°N, from NCEP–NCAR reanalysis data. Andes Mountains are indicated qualitatively in black.

Index (GPI), described below] for comparison with the 1998 simulations, supplemented by results from the Negri et al. (2002) technique for the year 2000.

This paper uses a 3-hourly infrared brightness temperature dataset from the GOES satellite on an 0.1° latitude–longitude grid spanning almost 2 yr (28 August 1998–30 June 2000). The eight times each day are 0245, 0545, . . . , 2345 UTC, which we abbreviate here as approximate local hours by subtracting 5 h, 45 min, yielding 2100, 0000, . . . , 1800 LT. For a few weeks during 1998, including the period of our model study (28 August–7 September) no images from 0545 UTC (local midnight) are available, owing to satellite maintenance operations. Care has been taken to minimize the impact of these missing data on results presented here.

Following Arkin and Meisner (1987), we plot the GPI, defined as the fractional coverage of brightness temperatures lower than 235 K, calibrated to rain-rate units using the constant factor 3 mm h^{-1}. Note that our usage pushes the GPI beyond its realm of calibrated validity, for example, by plotting small-scale patterns, and time averages at different times of day. Because of these concerns, Garreaud and Wallace (1997) omitted the 3 mm h^{-1} factor in their more extensive climatology of $<$235 K cloudiness. We favor rain-rate units in order to facilitate comparison to model precipitation, but because of the uncertainties involved we prefer this simple 3 mm h^{-1} factor to more complex calibrations, which would also be pushed beyond their range of proven validity by the small scales and time-of-day dependence considered here. Likely problems with the use of GPI include underestimation of rain from shallower clouds (e.g., orographic precipitation) and space and time offsets. The GPI data provide a delayed depiction of the diurnal cycle: upper-tropospheric anvil cloud coverage, and hence GPI, tends to lag surface rain rate, by about 3 h over Brazil, for example (Negri et al. 2002).

A check on the time-mean calibration of GPI for this season and region was performed by comparison with the Precipitation Estimation from Remotely Sensed Information using Artificial Neural Networks (PERSIANN; Sorooshian et al. 2000) product. The PERSIANN product converts infrared cloud-top observations to rain-rate units using a system trained with data from the (Tropical Rainfall Measurement Mission (TRMM)) microwave emission estimates. Relative to PERSIANN, GPI overestimates small rain amounts at the margins of heavier rainfall (not shown), consistent with the known tendency of anvil clouds with $<$235 K brightness temperatures to spill over a larger space–time region than the associated convective rainfall (Arkin and Meisner 1987). Meanwhile, higher rain rates are slightly underestimated by GPI. These biases tend to cancel, such that September monthly means over the region 10°S–26°N, 50°–110°W are 186 mm for PERSIANN and 160 mm for GPI. While recognizing its shortcomings, we use GPI mainly for its simplicity. The 2-yr period considered here is rather short to deserve the name ''climatology,'' but examination of other sources reveals it to be adequate to illustrate the basic seasonal and diurnal cycles, and put the 10-day period of our modeling efforts in context.

This paper also makes use of the very-high-resolution rain-rate estimates of Negri et al. (2002) for the year 2000. These data are also derived from infrared imagery, in this case hourly, in which convective and stratiform rain are identified using texture algorithms, and rain rate is calibrated with TRMM microwave estimates as well as South American rain gauge data. While the year 2000 is neither the year of our simulations, nor exactly representative of long-term climatology, the unprecedented quality and resolution of these data warrant their inclusion here. The climatological diurnal cycle is well captured in a single year's data.

4. Climatology of the region and season

The seasonal march of GPI in the American Tropics is shown in Fig. 2, in a linear gray scale (used in all such figures in this work) that makes the amount of ink on the page proportional to rainfall. The main rainfall zone migrates back and forth along a northwest–southeast track, from the eastern Pacific and Central American region during May–October to continental South America during November–April. The coastal concavity in the western Colombia/Gulf of Panama region (near 5°N, 78°W) is wet throughout the year, even in November–January (Fig. 2b). This coastal concavity is paralleled about 100 km inland by a concavity in the western branch of the Andes. A mean westerly wind at low levels is directed into this mountain barrier throughout the year (the ''Chocó jet''; Poveda and Mesa 2001), bringing moisture to the climatological maximum of rainfall. In every season, the rainfall of this region appears distinctly separated from the main mass of South American convective activity by the northern Andes.

Several interesting small-scale features are seen in the eastern Pacific in Fig. 2. For example, Fig. 2c shows a low-rainfall stripe along 80°W in February–April, separating GPI maxima on the Colombian coast and far offshore along 5°N. This dry stripe is present in all six of the monthly means entering Fig. 2c, and overlies a climatological cold stripe in sea surface temperature (SST, not shown), associated with a northerly surface wind jet through a gap in the topography near the Panama Canal. This jet is one of several intense topographically channeled gap winds from the Atlantic to the Pacific, especially in northern winter (Chelton et al. 2000). The local minimum in rainfall near 10°N, 90°W in northern summer (Figs. 2a, 2d) is also collocated with climatologically lower SST and higher wind speed than adjacent regions (not shown).

For arbitrary reasons, involving the availability of satellite and reanalysis data at the outset of this project, our modeling efforts have focused on the 10-day period from 28 August to 7 September. According to Fig. 2a,

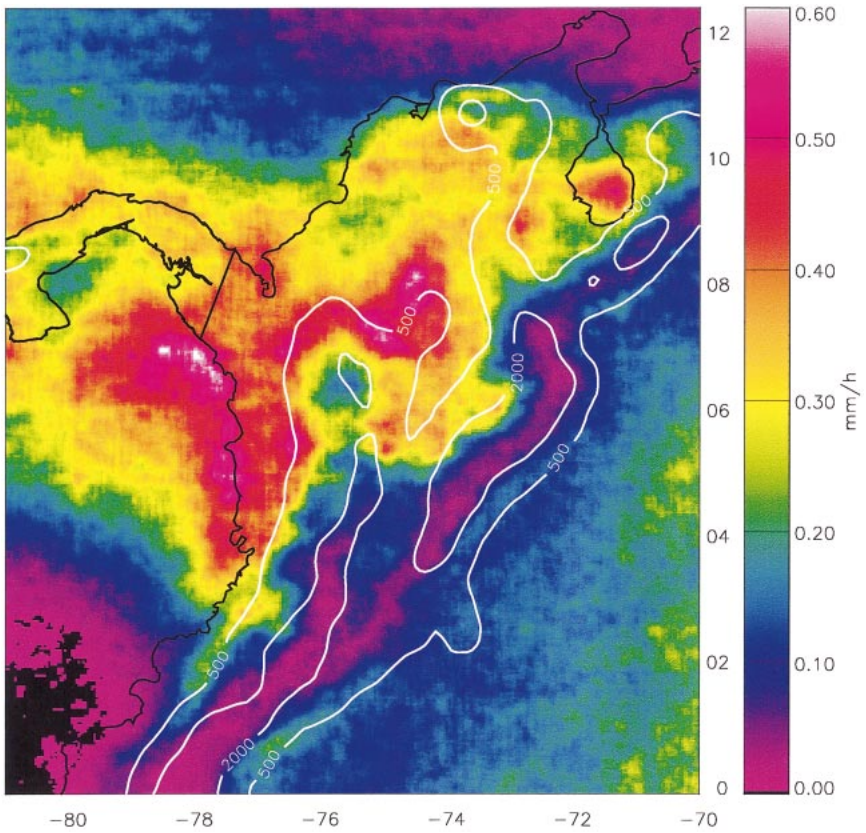

FIG. 6. Satellite-estimated annual mean rainfall rate for calendar year 2000, from the data of Negri et al. (2002). White curves indicate the 500- and 2000-m topographic contours.

this is the season when convection has the broadest spatial range in its occurrence, including large regions of the Atlantic basin as well as the eastern Pacific north of 5°N, and in a swath across South America. Even during this relatively wet part of the year, the eastern Caribbean (10°–16°N, 60°–75°W) has little rainfall. In this season, a strong low-level easterly jet blows across the Caribbean (Fig. 4), with divergence in the dry eastern basin and convergence in the wetter west. The associated Ekman drift leads to coastal upwelling along the northern coast of South America, causing climatological low SSTs under the regional minimum of GPI at 12°N, 66°W in Fig. 2a. Frictional divergence in the atmosphere also contributes to these dry conditions (Lahey 1973).

Figure 3 shows the long-term (1969–96) August plus September mean winds at 850- and 200-hPa levels, from the National Centers for Environmental Prediction (NCEP)–NCAR reanalysis (Kalnay et al. 1996). At 200 hPa (Fig. 3b), easterlies prevail from the equator through 10°N, especially over the Pacific, west of the divergence associated with the deep convective activity near the continent. Westerlies prevail in the Southern (winter) Hemisphere and over the northern subtropical Atlantic. At 850 hPa (Fig. 3a), easterlies prevail over almost the entire region, splitting into two streams west of 50°W: through the Caribbean (at 15°N) and up the Amazon Basin (on the equator). The westerly Chocó jet (Poveda and Mesa 2000) along 5°N in the eastern Pacific is the only westerly wind in Fig. 3a.

Low-level winds are depicted in more detail in Fig. 4, an August mean from the Sadler (1986) surface wind climatology. The westerlies of the Panama Bight region are depicted as recurved streamlines connected to the trade winds of the southeastern Pacific. The vertical structure of zonal wind along 5°N is shown in Fig. 5, again from the NCEP–NCAR reanalysis, with the Andes depicted as a solid black shape. The Chocó jet of low-level westerlies is seen to exist only below mountaintop level, overlain by easterlies at all levels.

5. Rainfall in western Colombia and the Panama Bight

Figure 6 shows a high-resolution annual mean rainfall estimate for 2000, based on the satellite estimates of Negri et al. (2002). The lowest values (black and purple) are seen over the equatorial eastern Pacific cold tongue, on the eastern (divergent) side of the Caribbean easterly jet of Fig. 4, and along the ridges of the high Andes, inside the white 2000-m topographic contour. To the southeast of the Andes, the rainfall is about 0.25 mm

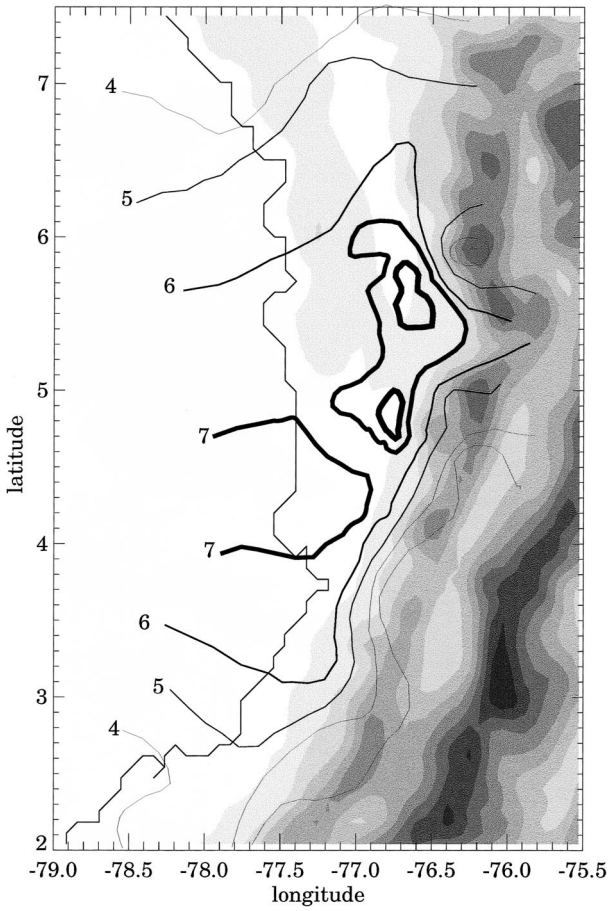

FIG. 7. Gauge climatology from Eslava (1994) of long-term mean rainfall in western Colombia. Shaded contours are topography (lightest shading at 200 m, then darker at 500 m and every 500 m thereafter). Open contours depict annual rainfall in m.

h^{-1} (2-m annual total), with little structure aside from a mean west–east gradient and the fine speckle reflecting the finite time sample. The rainfall structure is most interesting north and west of the Andes, with several maxima exceeding 0.5 mm h^{-1} along the white 500-m topographic contour. One notable feature is the maximum over Lake Maracaibo (10°N, 71°W), a shallow lake depicted in the land mask of Fig. 6. The greatest mean rainfall rates in the region (over 0.6 mm h^{-1}) lie immediately offshore of the Pacific coastline, as part of an offshore patch of high rainfall extending ~500 km along the coastline from 3.5° to 8°N. This offshore maximum is separated from the inland maxima near the 500-m contour by a relative minimum in the coastal lowlands.

A qualitative check on the accuracy and representativeness of the single-year satellite data is provided by a long-term rain gauge climatology for western Colombia, published by Eslava (1994), whose contours are reproduced in Fig. 7 on a shaded topographic map. Two areas with annual rainfall exceeding 7 m are indicated: one along the western Andes slopes from 4.5° to 6°N, and another region at the coastline, near 4°N where the coastline protrudes west into the Pacific. These data appear to support the picture of an offshore maximum (just barely detected by land-based gauges) and a separate inland maximum, with a relative minimum in the coastal plain. A more extensive gauge climatology of Colombian rainfall (G. Poveda 2002, personal communication) is in substantial agreement with Fig. 6, including the tendency for maximum rainfall at a low/intermediate elevation, and the structure of western Colombia rainfall in Fig. 7.

The diurnal cycle of the 2000 satellite data during the July–September season is shown in Fig. 8. Starting from 0000 LT (upper left), the rainfall increases along the Pacific coastline at 0200 and 0400 LT, and spreads offshore through the morning hours, weakening and propagating out of the plotted domain after local noon. Strong afternoon rainfall begins over the narrow isthmus of Panama at 1400 LT, with somewhat later development over continental South America. The climatological rainfall maximum at the foot of the western slopes of the Andes (noted in Figs. 6 and 7) can be seen to occur from 1600 to 2200 LT, weakening at midnight before the coastal rainfall begins developing strongly at 0200 LT.

Figure 8 also indicates that the climatological maximum of rainfall over the Magdalena valley of north-central Colombia (8°N, 75°W, see latitude–longitude labels in Fig. 6) has a diurnal cycle that peaks at 0200 LT. Nocturnal rainfall maxima over land occur in large, deep valleys in many parts of the world (e.g., Balling and Brazel 1987; Satomura 2000; Ohsawa et al. 2001). Lake Maracaibo also has the peak of its rainfall diurnal cycle at night. Nocturnal storms over Lake Maracaibo are so frequent that their lightning (known as the Lighthouse of Catatumbo) was used by Caribbean navigators in colonial times. Nocturnal convection occurs over other large tropical lakes, such as Lake Victoria (Flohn and Fraedrich 1966). Nocturnal rainfall can also be seen off the Caribbean coast of Panama in Fig. 8. After midnight, this rainfall increases, especially in the concavities of the coastline, and spreads farther offshore with time. There is also a sense of westward propagation, roughly in parallel with the westward propagation in the Pacific, crossing the western edge of the plotted region about noon.

Figure 9 indicates the approximate sizes of convective storms that contribute to the mean rainfall during the day and night. Each circle in Fig. 9 represents a contiguous region of cold cloud top with brightness temperature <210 K [obtained by a procedure detailed in Mapes and Houze (1993)], at the indicated local hour, sometime in the indicated 20-day period (which is centered on our 10-day simulation period). The size of the circle on the map is approximately equal to the cold-cloud area, although of course the real clouds are ragged and sometimes elongated or multilobed, not circular. In the afternoon (Fig. 9a), small circles crowd the northern

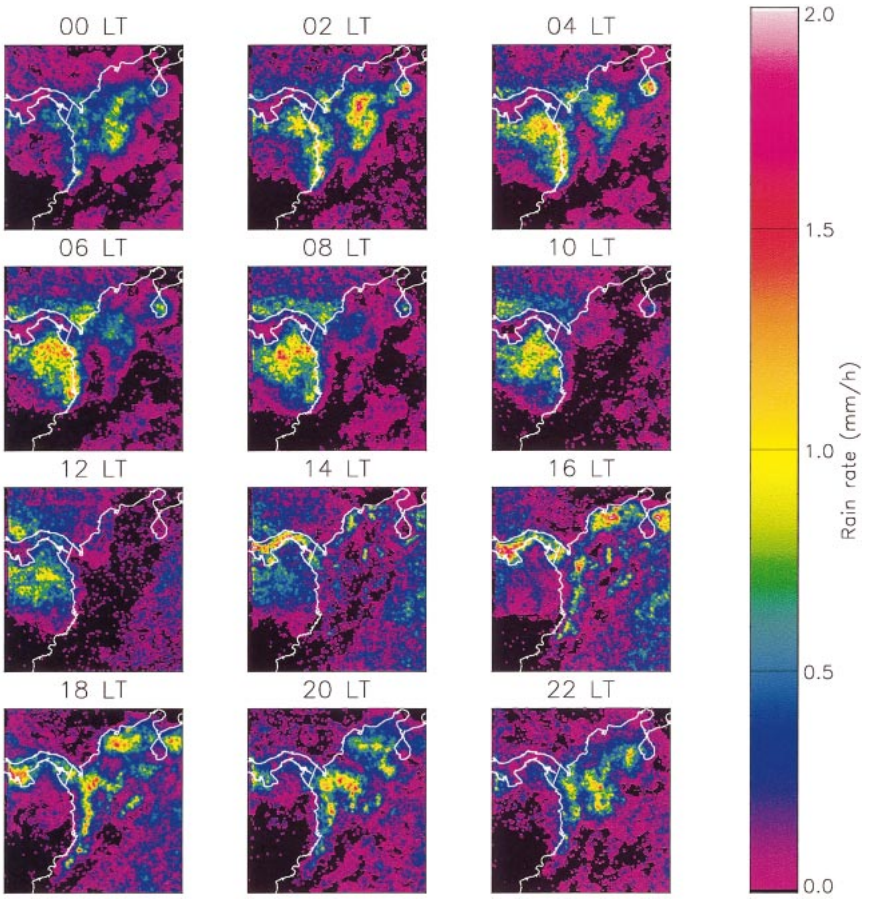

FIG. 8. Mean diurnal cycle of rainfall rate for Jul, Aug, and Sep of 2000 using the same data and plotting domain as in Fig. 6.

coast of South America and the Central American isthmus, while some larger circles can be seen over the Amazon. Near dawn (Fig. 9b), there are far fewer circles over the Amazon, but several are seen over land in the valleys of northern Colombia and the Lake Maracaibo area (not defined by land mask). Most of the cloudiness at this hour is seen to occur in larger systems off the Colombian coasts, both Pacific and Caribbean. Figure 9 makes the visual suggestion that the scale of the convective storms may be related to the scales of the geographic features in the area.

Mesoscale geographic features such as concave coastlines or mountains, subjected to diurnally cyclic heating, drive mesoscale atmospheric circulations. It is reasonable to suppose that these circulations can organize convection, encouraging the development of multicellular mesoscale convective systems. Such storms with scales of a few hundred kilometers have natural lifetimes (e.g., over the open ocean) approaching half a day (Chen et al. 1996; Chen and Houze 1997; Machado et al. 1998). For geographical concavities of this size, some sort of resonance may occur between diurnal forcing and the life cycle of mesoscale convective systems. High offshore rainfall in night/morning hours has been noticed in concave gulfs and bays worldwide (e.g., Neumann 1951; Houze et al. 1981; Negri et al. 1994; Ohsawa et al. 2001; Ricciardulli and Sardeshmukh 2002; Yang and Slingo 2001; Zuidema 2003), an observation that was an original motivation for this study. In many cases, it seems that the time of maximum rainfall is later for larger gulfs or bays, as in the case of the nocturnal maxima in Fig. 8. Interpretation is ambiguous in this case, however, since the later rainfall maximum in the larger, western concavity may reflect a westward propagation, as mentioned previously (and detailed extensively in Part III).

6. Is 10 days long enough to represent the seasonal climatology?

How long a period is necessary to justify interpreting the average of the weather as representative of the climate of the season? Given limited computing resources, the answer to this question determines the resolution, coverage, and suite of experiments that can be afforded in modeling studies. The details of our simulation tradeoffs are discussed more in Part II. Here we present evidence that 10 days is long enough to draw represen-

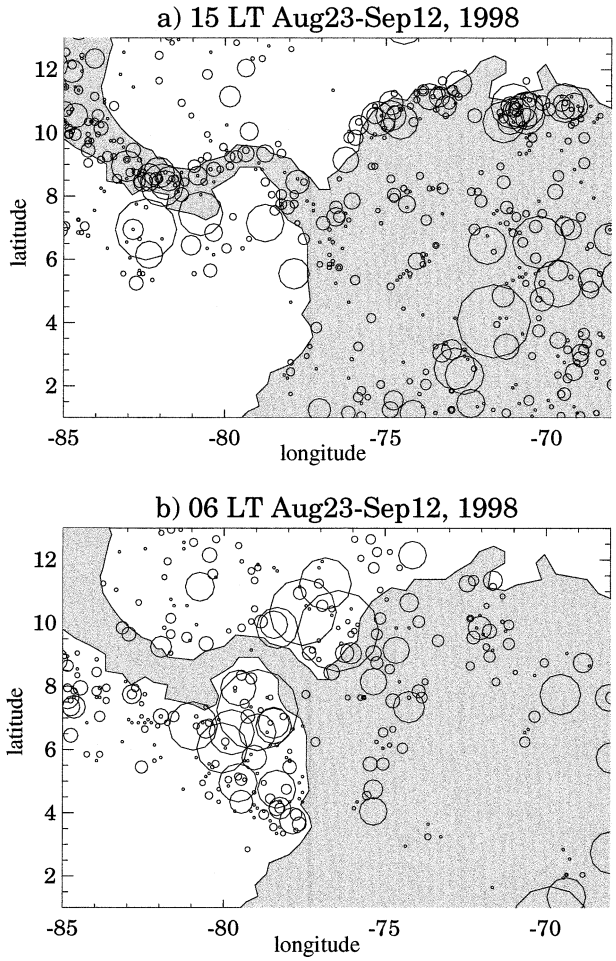

FIG. 9. Cloud clusters (contiguous regions of brightness temperature <210 K in 0.1° infrared satellite data) occurring during a 20-day period centered on the 10 days of our model study. Each circle is centered on the centroid point of a cloud cluster in one day's satellite image, with the size of the circle on the map equal to the area of the cloud cluster: (a) 1500 and (b) 0600 LT.

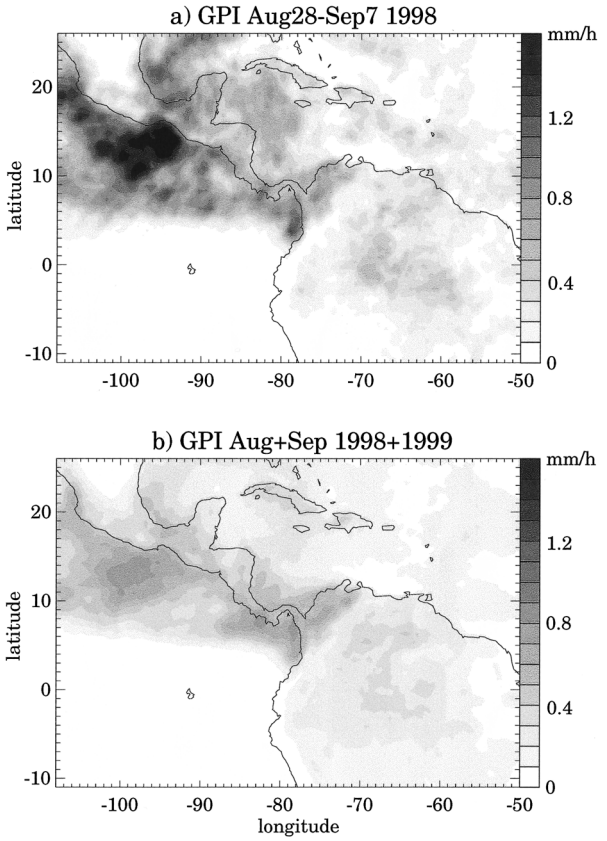

FIG. 10. Mean GPI maps for (a) 28 Aug–7 Sep 1998 and (b) Aug+Sep 1998+1999. Shading density is linearly proportional to rainfall.

tative conclusions about the climatological diurnal cycle in this region. This material also serves to place our 10-day period in its larger seasonal context.

The period of our simulations (28 August–7 September 1998) was chosen quite blindly, based on the availability of satellite data and reanalysis at the beginning of this work in 1998. It turns out to have been an active phase of intraseasonal variability, with unseasonably large rainfall and more and stronger organized convective disturbances, especially over the northern part of the domain. This may be seen by comparing time-mean GPI maps for our 10-day period (Fig. 10a) and for August plus September of 1998 and 1999 (Fig. 10b). The GPI pattern of the 10-day period resembles climatology, but with anomalously high values in the Caribbean Sea, Gulf of Mexico, and eastern Pacific. Domain average GPI in Fig. 10a is 1.3 times that in Fig. 10b.

Figure 11 shows time–longitude sections of GPI, averaged over the northern half of our largest model domain (8°–26°N, panel a) and the southern half (11°S–8°N, panel b), encompassing the time of our model work (indicated by boxes). Again it can be seen that 28 August–7 September was an unusually rainy period, especially in the northern part. In Fig. 11a, lines sloping up to the left indicate disturbances that traveled east to west, and apparently slowed down or accumulated in a massing of convective activity west of 90°W. These disturbances are known generically as easterly waves, and have been studied in this region in connection with east Pacific tropical cyclogenesis by Zehnder et al. (1999). Figure 11a indicates that the modeled period contains three distinct easterly waves. These three disturbances in close succession make the modeled period unusual within the season, again in the sense of more active weather. The eastern Pacific (longitudes −110° to −90°) is also seen to be in an enhanced phase of intraseasonal variation during the period of our simulations.

Figure 11b indicates westward moving disturbances in the southern part of the domain as well, but here the diurnal timescale is more dominant. Beginning at about 50°W, rainstorms developed in the afternoon and moved westward, sometimes persisting through the night and reintensifying the next day. These multiday propagating

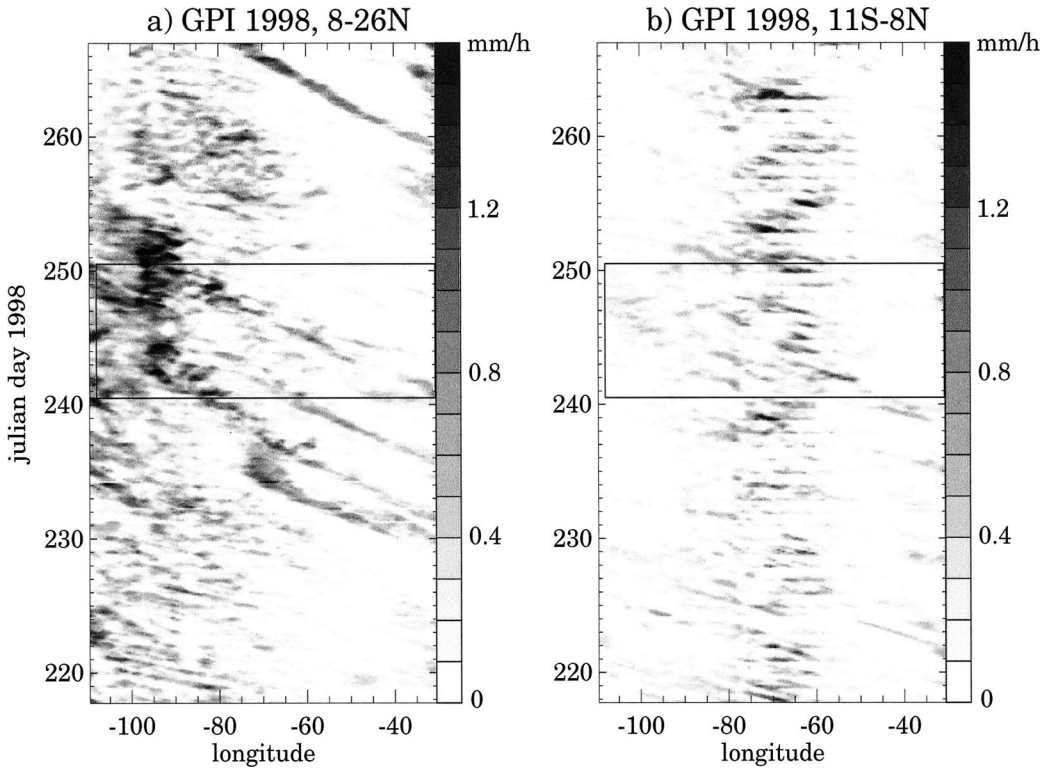

FIG. 11. Time–longitude sections of GPI averaged over the latitude bands (a) 8°–26°N and (b) 11°S–8°N. The time and largest space domain of our modeling study is indicated by boxes. Shading is linearly proportional to rainfall.

bands over the Amazon (e.g., Cohen et al. 1995), in combination with the general tendency for an afternoon rain maximum over land, leave their mark in long-term rainfall climatology as a banded structure parallel to the coast (Kousky 1980; Garreaud and Wallace 1997). Figure 11b also shows the westward-propagating convective storms that form near 77°W, off the west coast of Colombia. The day-to-day variability of these features appears incoherent with that of the disturbances over the Amazon.

Finer-scale time–longitude GPI rainfall plots for western Colombia are shown in Fig. 12. Figure 12a shows the composite diurnal cycle of August and September of 1998 and 1999, repeated twice for clarity, with the coastline and local midnight indicated by dashed and solid lines, respectively. Figure 12b shows the 10 simulated days, indicating 3 or 4 days with especially heavy rainfall on the western side of the Andes (the mountain profile in longitude is indicated outside the plot boxes). Recall that the GPI rainfall estimate tends to give a delayed, and perhaps distorted, depiction of the diurnal cycle. The rainfall over coastal land peaks a few hours before midnight, with tilted contours indicating a tendency for slow motion toward and across the coastline. After midnight, convection develops strongly and suddenly over the ocean, sharply bounded by the coastline. Rainfall over the water propagates westward through the daytime hours, steadily weakening. A second region of after-midnight rainfall is seen in the Cauca–Magdalena valley, the central valley of the (latitudinally averaged) Andes profile. All these features have already been described in connection with Fig. 8.

In summary, the 10-day period of our model studies had more active weather than the 1998–99 climatology (more rain in domain average, more and stronger easterly disturbances in the Atlantic and Caribbean, and more rain in the Panama Bight). It should also be noted that August–September 1998 was in the late stage of the strong 1997–98 El Niño event. Interannual anomalies of sea surface temperature were up to +5 K in the cold tongue just south of the equator (see Fig. 1), and +1 to +2 K in the Panama Bight latitudes near 5°N. Consistent with the warmer water, deep convection and low-level zonal wind also had positive interannual anomalies in the far eastern Pacific during August–September 1998. Thus our study period was doubly anomalous, all in the sense of more active weather. Still, the spatial pattern of rainfall and the underlying weather phenomenology are sufficiently representative that the physical processes identified in this work may be con-

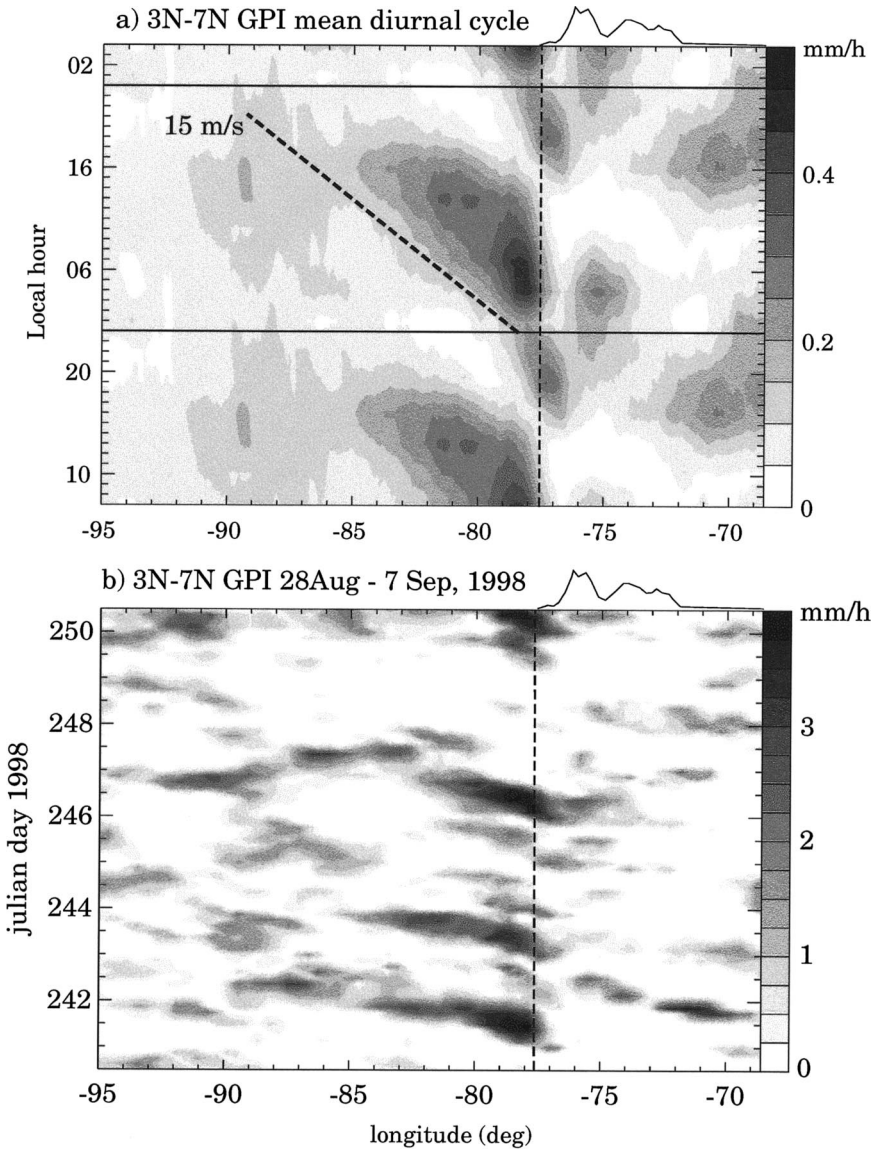

FIG. 12. Time–longitude sections of GPI for western Colombia, averaged over the latitude band 3°–7°N. (a) The composite mean diurnal cycle for all available data from Aug and Sep of 1998 and 1999, repeated twice for clarity. (b) The 10 days of the model study. Shading density is linearly proportional to rainfall. The profile of the Andes in this latitude belt is indicated by the jagged curves atop the plot boxes. Vertical dashed lines indicate the coast; horizontal solid lines in (a) indicate local midnight.

sidered typical of those that shape the seasonal climatology of the region.

7. Summary and conclusions

Observational context for the mesoscale model results of Parts II and III has been presented, beginning with the seasonal march of convection and rainfall in the region. Rainfall generally follows the sun between the hemispheres, with northern summer rainfall being maximal in the eastern Pacific and southern summer rainfall over the Amazon basin. Northwestern South America sits at the center of this northwest–southeast annual march, such that the Panama Bight region is wet throughout the year. In southern summer, rainfall in this region appears disconnected by the Andes from the main continental-scale monsoon (Figs. 2b,c), while in northern summer it is contiguous with the ITCZ north of the equator. There is a steep meridional gradient of rainfall along the west coast of South America, paralleling the steep meridional gradient of sea surface temperature offshore, in the northern edge of the eastern equatorial

Pacific cold tongue. Within Colombia, the rainfall pattern is quite complex, with maximum values tending to lie along the 500-m topographic contour (Fig. 6).

The diurnal cycle of rainfall also generally has rain following the sun, with convection developing over land during the afternoon (Fig. 8). Much of the daytime convection takes the form of small cloud systems, especially in coastal zones and the narrow isthmus of Central America, although larger systems do develop over the Amazon (Fig. 9a). Nocturnal rainfall is observed offshore and tends to propagate away from land through the night and morning hours. Much of the offshore convection occurs as contiguous convective cloud systems with scales similar to those of the geography (Fig. 9b). Nocturnal convection also occurs in the valleys of Colombia and over Lake Maracaibo. Over the Amazon basin, diurnally generated convection tends to propagate westward, with systems sometimes lasting 2–3 days and crossing the entire Amazon basin (Cohen et al. 1995). West of the Andes, in the Panama Bight, a distinctive westward-propagating diurnal rain pattern is also seen (Fig. 12), but the day-to-day variability of this appears incoherent with that of the Amazon diurnal bands (Fig. 11b). The low-level wind is easterly over the Amazon, with a speed comparable to the propagation speed of the diurnal rainbands, but is westerly over the Panama Bight (Fig. 5), where the mechanism of propagation appears to involve gravity waves (Part III).

More detailed climatological data were examined for the August–September season, and for the specific 10-day period simulated in this study (28 August–7 September, 1998). This 10-day period had unseasonably active weather, especially in the northern half of our largest model domain, with three prominent easterly disturbances in the Atlantic–Caribbean basin and an enhanced intraseasonal massing of deep convection in the eastern Pacific (Fig. 11a). Still, the 10-day mean rainfall spatial pattern strongly resembles a longer-term mean (Fig. 10), suggesting that the processes that shape the rainfall of our 10-day simulation period are adequately representative of the processes that shape the longer-term climatology.

Acknowledgments. This research was supported by the NOAA Office of Global Programs, under the Pan-American Climate Studies (PACS) program, Grant NA96GP0051. The infrared satellite data for the GPI rainfall estimates were kindly supplied by the PACS project of Drs. John Bates and Wesley Berg. German Poveda, Jorge Ramirez, Saul Marin, Jose Lino Jurado Montano, and David Enfield enriched our understanding and appreciation of the fascinating hydroclimate of Colombia and the Panama Bight. The constructive criticisms of two anonymous reviewers greatly improved this manuscript.

REFERENCES

Adler, R. F., G. J. Huffman, D. T. Bolvin, S. Curtis, and E. J. Nelkin, 2000: Tropical rainfall distributions determined using TRMM combined with other satellite and rain gauge information. *J. Appl. Meteor.*, **39,** 2007–2023.

Arkin, P. A., and B. N. Meisner, 1987: The relationship between large-scale convective rainfall and cold cloud over the Western Hemisphere during 1982–84. *Mon. Wea. Rev.*, **115,** 51–74.

Balling, R. C., Jr., and S. W. Brazel, 1987: Diurnal variations in Arizona monsoon precipitation frequencies. *Mon. Wea. Rev.*, **115,** 342–346.

Carbone, R. E., J. D. Tuttle, D. A. Ahijevych, and S. B. Trier, 2002: Inferences of predictability associated with warm season precipitation episodes. *J. Atmos. Sci.*, **59,** 2033–2056.

Chelton, D. B., M. H. Freilich, and S. K. Esbensen, 2000: Satellite observations of the wind jets off the Pacific coast of Central America. Part I: Case studies and statistical characteristics. *Mon. Wea. Rev.*, **128,** 1993–2018.

Chen, S. S., and R. A. Houze Jr., 1997: Diurnal variation and life-cycle of deep convective systems over the tropical Pacific warm pool. *Quart. J. Roy. Meteor. Soc.*, **123,** 357–388.

——, ——, and B. E. Mapes, 1996: Multiscale variability of deep convection in relation to large-scale circulation in TOGA COARE. *J. Atmos. Sci.*, **53,** 1380–1409.

Cohen, J., M. Silva Dias, and C. Nobre, 1995: Environmental conditions associated with Amazon squall lines: A case study. *Mon. Wea. Rev.*, **123,** 3163–3174.

Day, P. C., 1926: Climatological data for Andagoya, Republic of Colombia, South America. *Mon. Wea. Rev.*, **54,** 376–378.

Eslava, J. A., 1994: Acerca de la distribucion espacio-temporal de la precipitation en la region del pacifico Colombiano. *Atmosfera*, **22,** 71–80.

Figueroa, S. N., and C. A. Nobre, 1990: Precipitation distribution over central and western tropical South America. *Climanálise*, **5,** 36–45.

Flohn, H., and K. Fraedrich, 1966: Tagesperiodische zirkulation und niederschlagsverteilung am Victoria-See (Ostafrika). *Meteor. Rundsch.*, **19,** 157–165.

Forsbergh, E. D., 1969: On the climatology, oceanography, and fisheries of the Panama Bight. Inter-American Tropical Tuna Commission Bulletin, Vol. 14, No. 2, 49–219.

Garreaud, R. D., and J. M. Wallace, 1997: The diurnal march of convective cloudiness over the Americas. *Mon. Wea. Rev.*, **125,** 3157–3171.

Horel, J. D., and A. G. Cornejo-Garrido, 1986: Convection along the coast of northern Peru during 1983: Spatial and temporal variation of clouds and rainfall. *Mon. Wea. Rev.*, **114,** 2091–2105.

——, A. N. Hahmann, and J. E. Geisler, 1989: An investigation of the annual cycle of convective activity over the tropical Americas. *J. Climate*, **2,** 1388–1403.

Houze, R. A., Jr., S. Geotis, F. Marks, and A. West, 1981: Winter monsoon convection in the vicinity of north Borneo. Part I: Structure and time variation of the clouds and precipitation. *Mon. Wea. Rev.*, **109,** 1595–1614.

Kalnay, E., and Coauthors, 1996: The NCEP/NCAR 40-Year Reanalysis Project. *Bull. Amer. Meteor. Soc.*, **77,** 437–471.

Kousky, V., 1980: Diurnal rainfall variation in northeast Brazil. *Mon. Wea. Rev.*, **108,** 488–498.

Lahey, J. F., 1973: On the origin of the dry climate in northern South America and the southern Caribbean. *Coastal Deserts: Their Natural and Human Environments*, D. H. K. Amiran and A. W. Wilson, Eds., The University of Arizona Press, 75–90.

Machado, L. A. T., W. B. Rossow, R. L. Guedes, and A. W. Walker, 1998: Life cycle variations of mesoscale convective systems over the Americas. *Mon. Wea. Rev.*, **126,** 1630–1654.

Mapes, B. E., and R. A. Houze Jr., 1993: Cloud clusters and superclusters over the oceanic warm pool. *Mon. Wea. Rev.*, **121,** 1398–1416.

——, T. T. Warner, and M. Xu, 2003: Diurnal patterns of rainfall in northwestern South America. Part III: Diurnal gravity waves and nocturnal convection offshore. *Mon. Wea. Rev.*, **131,** 830–844.

Meisner, B. N., and P. A. Arkin, 1987: Spatial and annual variations

in the diurnal cycle of large-scale tropical convective cloudiness and precipitation. *Mon. Wea. Rev.*, **115,** 2009–2030.

Mesa, O. J., G. Poveda, and L. F. Carvajal, 1997: *Introduction al clima de Colombia*. Universidad Nacional de Colombia, 390 pp.

Negri, A. J., R. F. Adler, E. J. Nelkin, and G. J. Huffman, 1994: Regional rainfall climatologies derived from Special Sensor Microwave Imager (SSM/I) data. *Bull. Amer. Meteor. Soc.*, **75,** 1165–1182.

——, L. Xu, and R. F. Adler, 2002: A TRMM-calibrated infrared rainfall algorithm applied over Brazil. *J. Geophys. Res.*, **107** (D20), 8048, doi:10.1029/2000JD000265.

Neumann, J., 1951: Land breezes and nocturnal thunderstorms. *J. Meteor.,* **8,** 60–67.

Nichols, J. T., and R. C. Murphy, 1944: A collection of fishes from the Panama Bight, Pacific Ocean. *Amer. Mus. Nat. Hist. Bull.*, **83,** 217–260.

Ohsawa, T., H. Ueda, T. Hayashi, A. Watanabe, and J. Masumoto, 2001: Diurnal variations of convective activity and rainfall in tropical Asia. *J. Meteor. Soc. Japan*, **79,** 333–352.

Poveda, G., and O. J. Mesa, 2000: On the existence of Llorø (the rainiest locality on Earth): Enhanced ocean–land–atmosphere interaction by a low-level jet. *Geophys. Res. Lett.,* **27,** 1675–1678.

Ricciardulli, L., and P. D. Sardeshmukh, 2001: Local time–space and scales of tropical deep convection. *J. Climate*, **15,** 2775–2790.

Sadler, J. C., 1986: Analysis strategy for COADS and some comparison of products. *Proc. COADS Workshop*, Boulder, CO, NOAA Tech. Memo. ERL ESG-23, 116–120.

Satomura, T., 2000: Diurnal variation of precipitation over the Indo-China peninsula: Two-dimensional numerical simulation. *J. Meteor. Soc. Japan*, **78,** 461–475.

Snow, 1976: The climate of northern South America. *Climates of Central and South America*, W. Schwerdtfeger, Ed., World Survey of Climatology, Vol. 12, Elsevier, 295–403.

Sorooshian, S., K.-L. Hsu, X. Gao, H. V. Gupta, B. Imam, and D. Braithwaite, 2000: Evaluation of PERSIANN system satellite-based estimates of tropical rainfall. *Bull. Amer. Meteor. Soc.*, **81,** 2035–2046.

Trewartha, G. T., 1981: *The Earth's Problem Climates*. University of Wisconsin Press, 366 pp.

Velasco, I., and M. Fritsch, 1987: Mesoscale convective complexes in the Americas. *J. Geophys. Res.*, **92,** 9591–9613.

Wallace, J. M., 1975: Diurnal variations in precipitation and thunderstorm frequency and precipitation over the conterminous United States. *Mon. Wea. Rev.*, **103,** 406–419.

Warner, T. T., B. E. Mapes, and M. Xu, 2003: Diurnal patterns of rainfall in northwestern South America. Part II: Model simulations. *Mon. Wea. Rev.*, **131,** 813–829.

Xie, P., and P. A. Arkin, 1996: Analyses of global monthly precipitation using gauge observations, satellite estimates, and numerical model predictions. *J. Climate*, **9,** 840–858.

Yang, G.-Y., and J. Slingo, 2001: The diurnal cycle in the Tropics. *Mon. Wea. Rev.*, **129,** 784–801.

Zehnder, J. A., D. M. Powell, and D. L. Ropp, 1999: The interaction of easterly waves, orography, and the intertropical convergence zone in the genesis of eastern Pacific tropical cyclones. *Mon. Wea. Rev.*, **127,** 1566–1585.

Zuidema, P., 2003: Convective clouds over the Bay of Bengal. *Mon. Wea. Rev.*, **131,** 780–798.